ORIGINAL PAPER

Cohesive crack, size effect, crack band and work-of-fracture models compared to comprehensive concrete fracture tests

Christian G. Hoover · Zdeněk P. Bažant

Abstract The simplest form of a sufficiently realistic description of the fracture of concrete as well as some other quasibrittle materials is a bilinear softening stress-separation law (or an analogous bilinear law for a crack band). This law is characterized by four independent material parameters: the tensile strength, f_t', the stress σ_k at the change of slope, and two independent fracture energies—the initial one, G_f and the total one, G_F. Recently it was shown that all of these four parameters can be unambiguously identified neither from the standard size effects tests, nor from the tests of complete load-deflection curve of specimens of one size. A combination of both types of test is required, and is here shown to be sufficient to identify all the four parameters. This is made possible by the recent data from a comprehensive test program including tests of both types made with one and the same concrete. These data include Types 1 and 2 size effects of a rather broad size range (1:12.5), with notch depths varying from 0 to 30 % of cross section depth. Thanks to using identically cured specimens cast from one batch of one concrete, these tests have minimum scatter. While the size effect and notch length effect were examined in a separate study, this paper deals with inverse finite element analysis of these comprehensive test data. Using the crack band approach, it is demonstrated: (1) that the bilinear cohesive crack model can provide an excellent fit of these comprehensive data through their entire range, (2) that the G_f value obtained agrees with that obtained by fitting the size effect law to the data for any relative notch depth deeper than 15 % of the cross section (as required by RILEM 1990 Recommendation), (3) that the G_F value agrees with that obtained by the work-of-fracture method (based on RILEM 1985 Recommendation), and (4) that the data through their entire range cannot be fitted with linear or exponential softening laws.

Keywords Scaling · Strength · Fracture energy · Quasibrittle fracture · Nonlinear fracture mechanics

C. G. Hoover
Northwestern University, Evanston, IL, USA

Present address:
C. G. Hoover
M.I.T., Cambridge, MA, USA

Z. P. Bažant (✉)
Northwestern University, 2145 Sheridan Road, CEE/A135, Evanston, IL 60208, USA
e-mail: z-bazant@northwestern.edu

1 Introduction

Modeling of the fracture of concrete has been impeded by the unavailability of a comprehensive database for fracture of one and the same concrete. Although a vast number of fracture data exist in the literature (Bažant and Becq-Giraudon 2002; Rocco 1995; Sabnis and Mirza 1979; Bažant and Planas 1998; Malvar and Warren 1988; Nallathambi 1986; Petersson 1981; Carpinteri et al. 1995; Bažant and Pfeiffer 1987; Tang et al.

1996; Karihaloo et al. 2003), they are all rather limited in scope, have limited specimen size ranges, geometries and post peak information, and have been performed on different concretes or different batches of supposedly the same concrete, at different ages, under different environmental conditions, at different rates, with different test procedures, and on specimens of different types and dimensions. In a combined data set, the interpretation suffers by ambiguity since the fracture behavior is obscured by the differences in all the aforementioned features. Thus it is not surprising that some very different models, with weak experimental validations, have co-existed for a long time. Arguments favoring one model or another have undermined confidence in fracture mechanics among practicing engineers and in the committees responsible for updating the design code.

To generate a more useful database with unambiguous interpretation, the U.S. Department of Transportation funded a large fracture testing program, the most comprehensive so far. The specimens were cast from the same batch of a normal-strength concrete, were subjected to the same curing conditions and were tested at the same curing age. Sets of beams of 18 different geometries were used. Altogether, tested were 140 beams with the size range of 1:12.5 and with relative notch depths ranging from 0 to 30 % of the beam depth. All but five of them gave a stable postpeak softening response, extended to as low as 10 % of the peak load in most cases, and 5 % in a few cases. These data have recently been reported in Hoover et al. (2013). In Hoover and Bažant (2013), they were then used to study the laws of size effect and crack length effect and in Hoover and Bažant (2014a,b) they were used to validate a new universal law for the effects of size and crack depth combined.

The objective of this paper is to verify: (1) whether the finite element analysis with the well-known cohesive crack model can describe these test results, (2) whether the fracture parameters obtained by finite element fitting of the test data by the crack band model are in agreement with those obtained by fitting of the test data for different relative notch depths by the size effect law, and (3) whether the bilinear softening is needed to fit all the data. Previous attempts with a similar objectives were made in Yu et al. (2010), but they led to weak conclusions since they had to rely on a much more limited collection of tests from the literature which were not directly comparable and had rather limited scopes.

2 Review of size effect

The nominal strength of geometrically similar structures is a parameter of the maximum load having the dimension of stress, defined as

$$\sigma_N = c_N \frac{P_u}{bD} \tag{1}$$

where D = structure size (or characteristic dimension), P_u = maximum applied load (or load capacity), b = structure width, and c_N = dimensionless constant chosen for convenience. According to the classical theories of elasticity and plasticity, which still form the basis of the American Concrete Institute (ACI) design code and most other codes, the nominal strength of a structure is independent of D. Thus the size effect is understood as any dependence of σ_N on D. The size effect is a very important attribute of quasibrittle (or cohesive softening) fracture mechanics and damage mechanics (Bažant and Planas 1998).

When the classical linear elastic fracture mechanics (LEFM) is applied to geometrically similar perfectly brittle structures with geometrically similar cracks, the size effect is $\sigma_N \propto D^{-1/2}$, which is the strongest possible. For quasibrittle materials, such as concrete, ceramics, rocks, sea ice, wood, fiber composites, stiff foams and bone, one can distinguish two simple types of size effect. The type 2 size effect is exhibited by geometrically similar structures that contain, at maximum load, cracks or notches that are not negligible compared to the size of cross section of structure and are sufficiently larger than the fracture process zone (FPZ). This type of size effect is of energetic (non-statistical) origin and is transitional between plasticity and LEFM. It is approximately described by the size effect law (Bažant 1984):

$$\sigma_N = \frac{Bf'_t}{\sqrt{1 + D/D_0}} \quad \text{(Type 2)} \tag{2}$$

Here f'_t = tensile strength of concrete, introduced for convenience of dimension; B = dimensionless parameter characterizing the geometry; D_0 = transitional structure size; B and D_0 can be identified by fitting the test data or simulations by the cohesive crack model. The transitional behavior is caused by the fact that the FPZ size, equal to several inhomogeneity sizes, is not negligible compared to the cross section dimension.

Equation (2) was derived Bažant (1984) by simple energy release analysis and later by several other ways, especially by asymptotic matching based on the asymptotic power scaling laws for very large and very small

Fig. 1 Dependence of σ_N on size D of beams with no notch (*left*) and deep notch (*right*)
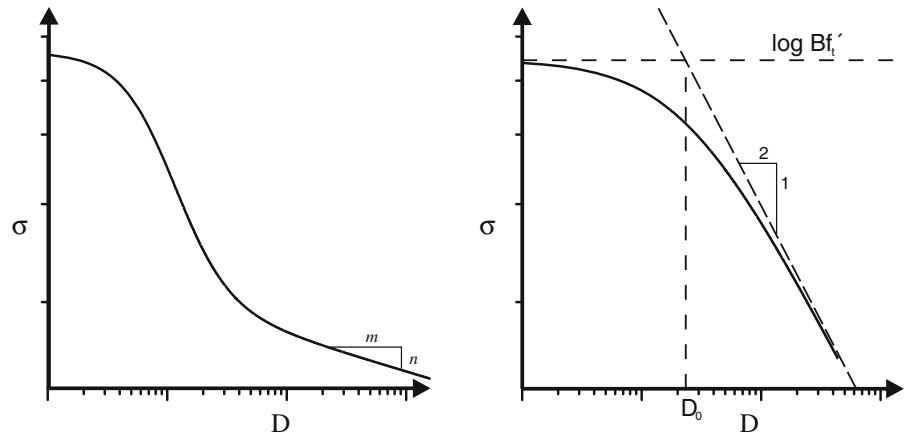
D (Bažant and Planas 1998; Bažant 2005). The size effect is best shown in the plot of $\log \sigma_N$ versus $\log D$. When geometrically similar beams with a broad size range contain deep notches or pre-existing stress-free (or fatigued) cracks of large depth a relative to structure size D, the size effect is of Type 2. This type represents a smooth transition from a horizontal line for small sizes (corresponding to plasticity or strength theory) to an inclined asymptote of slope $-1/2$ for large sizes (corresponding to LEFM) (Fig. 1 right).

By means of asymptotic matching, the coefficients of Eq. (2) have been shown (Bažant and Kazemi 1991) to be approximately related to the LEFM fracture characteristics as follows:

$$\sigma_{Nu} = \sqrt{\frac{E' G_f}{g(\alpha_0)D + g'(\alpha_0)c_f}} \qquad (3)$$

where $\alpha = a/D$ = relative crack length, $\alpha_0 = a_0/D$ = initial value of α, a_0 = notch depth; $E' = E$ = Young's modulus for plane stress and $E' = E/(1-\nu^2)$ for plane strain (where ν = Poisson ratio) and G_f = initial fracture energy = area under the initial tangent of the cohesive softening stress-separation law. The dimensionless energy release rate function of LEFM, $g(\alpha_0)$, and its derivative and $g'(\alpha_0) = \mathrm{d}g(\alpha_0)/\mathrm{d}\alpha_0$ are calculated from $g(\alpha_0) = k^2(\alpha_0)$ and $k(\alpha_0) = b\sqrt{D}K_I/P$ where K_I = stress intensity factor and P = load. The effective FPZ length c_f is related to Irwin's characteristic length l_0 (Irwin 1958) as $c_f = \gamma l_0$ where, for the present span-to-depth ratio, $\gamma = 0.29$ (if $0.15 \le \alpha_0 \le 0.6$) (Bažant and Yu 2011; Cusatis and Schauffert 2009). Rearranging Eq. (3), one may show that:

$$B f_t' = E' G_f/g_0' c_f, \quad D_0 = c_f g_0'/g_0 \qquad (4)$$

Note that the LEFM function $g(\alpha_0)$ or $k(\alpha_0)$ embodies information on the effects of both the structure size and the relative crack length, the latter being the effect of structure geometry or shape. In Bažant and Pfeiffer (1987), it was further shown that separate fitting of Eq. (3) to the size effect data for three-point bend, eccentric compression, and double-edge-notched tension specimens yields about the same G_f. Thus Eq. (3) is not only a size effect law but also a size-shape effect law for Type 2 failures.

The Type 1 size effect is observed in structures of the so-called positive geometry (Bažant and Planas 1998) that fail under controlled load as soon as the macrocrack initiates from a smooth surface. The deterministic Type 1 size effect law reads (Fig. 1 left):

$$\sigma_N = f_{r\infty} \left[1 + \frac{r D_b}{D + l_p} \right]^{1/r} \quad \text{(Type 1)} \qquad (5)$$

Here $f_{r\infty}$, D_b, l_p and r are empirical constants to be determined from tests; D_b = depth of the boundary layer of cracking (roughly equal to the FPZ size), $f_{r\infty}$ = nominal strength for very large structures (when the Weibull statistical size effect is negligible), l_p = material characteristic length that is related to the maximum aggregate size. Note that l_p differs from Irwin's characteristic length $l_0 = E G_f/f_t^2$ (Irwin 1958), which characterizes the FPZ length in the direction of propagation.

In contrast to Type 2, Eq. (5) for Type 1 terminates at $D \to \infty$ with a horizontal asymptote, provided that the Weibull statistical size effect (Weibull 1939, 1951) is negligible. In general, the Type 1 size effect can have a statistical Weibull component (Bažant and Novák 2000; Bažant 2005), but for three-point bend beams, this component is negligible, which is one

reason for choosing such beams. Why negligible?—because the zone of high stress is rather concentrated, even in absence of a notch. This prevents the critical crack from forming at widely different locations of different random local strength (for the same reason, the statistical size effect on the mean strength is negligible in Type 2 failures, too).

When the crack at failure is neither negligible nor large, the size effect trend is a transition between the Types 1 and 2. A new combined, or 'universal', size-shape effect law was derived in terms of the strain gradient at the smooth surface and then compared to the comprehensive fracture tests in (Hoover and Bažant 2014b). It improved on two previous universal laws which were attempted purely theoretically, in absence of good test data (Bažant 1996; Bažant and Li 1996; Bažant and Yu 2004, 2009). The new universal size effect law (USEL) has two forms, depending on whether or not there is a statistical component. The nonstatistical form of USEL is as follows:

$$\sigma_N = \left(\frac{E'G_f}{g_0 D + (1-\lambda)c_f g_0' + \lambda E'G_f/f_{r\infty}^2} \right)^{1/2}$$
$$\times \left[1 + \frac{r\lambda D_b}{\bar{D} + l_p} \right]^{1/r} \tag{6}$$

in which

$$\bar{D} = \frac{2\epsilon}{\psi \langle \epsilon_{,n} \rangle} \tag{7}$$

Here ψ, which is a geometry factor that depends on the beam span to depth ratio and is calculated from the strain profile, is equal to 0.896 (Hoover and Bažant 2014b) for the present beams. A Type 1–2 transition parameter is defined as

$$\lambda = e^{-\alpha_0^k (\bar{D}/d_a)^p / q} \tag{8}$$

where k, p and q are empirically fitted parameters, and d_a = maximum aggregate size. The transition parameter varies from $\lambda = 1$ for no-notch specimens to $\lambda = 0$ for deep notch specimens.

3 Damage evolution and cohesive softening law for crack band model

The test beams were analyzed under the assumption of plane stress using an open-source object-oriented finite element code called OOFEM (obtainable from www.oofem.org) (Patzák and Bittnar 2001).

Table 1 Size of elements in the middle of the beam, measured perpendicularly to the crack opening direction

Depth (mm)	Element size (mm)
40	3.84
93	8.92
215	6.88
500	16

The mesh consisted of rectangles and triangles with linear interpolation functions. The elements near the center of the beam, where the crack is expected to form, were smaller. Table 1 shows the mesh size, orthogonal to the direction of crack propagation. The element transitioned to a larger size closer to the supports.

All the simulations used the average beam thickness as measured on the actual test specimens (it differed only slightly from the design thickness of 1.58 in. or 40 mm). Two steel support blocks and one steel loading block were glued to concrete by cyanoacrylate ('superglue'). They were in the simulations connected at nodes to the concrete beam (Fig. 2). The steel was modeled as a linear elastic isotropic material with Young's modulus $E = 200$ GPa and Poisson's ratio $\nu = 0.30$.

The concrete in the transitional and larger elements was considered to be isotropic and linearly elastic, with the same E and ν as the concrete in the small elements before fracturing. The damage in all the smaller elements near the center of the beam was described by Mazars' isotropic damage model (Mazars 1984):

$$\sigma_{ij} = (1-\omega)C_{ijkl}\epsilon_{kl} \tag{9}$$

where C_{ijkl} = elastic stiffness tensor; $\sigma_{ij}, \epsilon_{ij}$ = stress and strain tensors; ω = damage parameter varying from 0 to 1; and the subscripts refer to cartesian coordinates x_i ($i = 1, 2, 3$). The damage parameter was assumed to depend on a history variable, κ, which characterizes the maximum strain magnitude that the material at the given point has experienced so far; ω increases as κ increases, and remains unchanged if κ decreases or remains constant.

The assumption of isotropy of damage, which is what makes Mazars' model simple, would be unrealistic for a field of oriented distributed cracking but, when the cracking is localized into a narrow band, the orientation of cracking within the band is unimportant and

Fig. 2 Examples of mesh for $D = 93$ mm beams. *Left* For $\alpha = 0.3$; *Right* for no notch
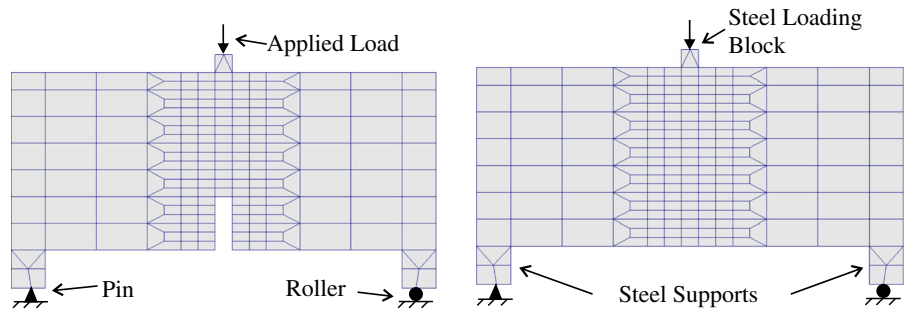
Fig. 3 Bilinear softening law in terms of stress versus strain (*left*) and versus opening displacement (*right*)
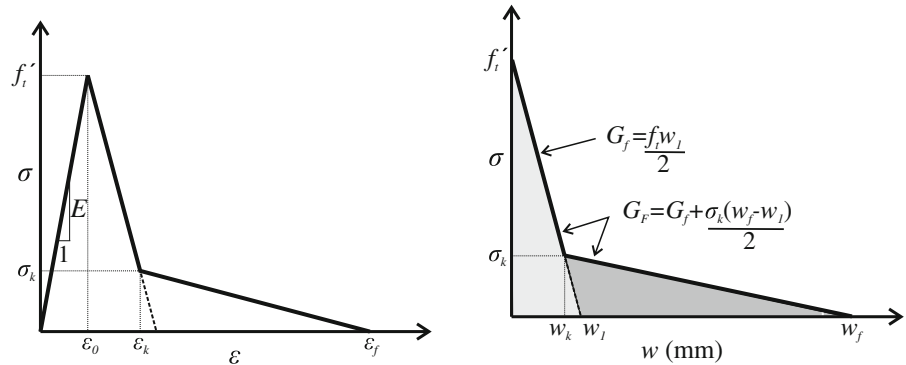
the only thing that matters is how the normal stress across the band softens with increasing strain across the band.

To describe the softening function that characterizes the evolution of damage parameter ω with the tensile strain magnitude κ, a linear function up to the peak, followed in post-peak by a downward shifted exponential function, was proposed originally by Hillerborg. But later it was found to be insufficient to match broader sets of experimental curves. The simplest, yet realistic, softening function is the bilinear function. It is expressed in terms of a bilinear stress-separation law of a crack, which may be conveniently approximated by a similar law for the evolution of damage in a crack band with smeared cracking;

$$\omega(\kappa) = \begin{cases} 0 & (\kappa < \epsilon_0) \\ 1 - \frac{E\epsilon_0(\epsilon_k - \kappa) + \sigma_k(\kappa - \epsilon_0)}{E\kappa(\epsilon_k - \epsilon_0)} & (\epsilon_0 \le \kappa \le \epsilon_k) \\ 1 - \frac{\sigma_k}{E\kappa} \frac{\epsilon_f - \kappa}{\epsilon_f - \epsilon_k} & (\epsilon_k \le \kappa \le \epsilon_f) \\ 1 & (\kappa > \epsilon_f) \end{cases} \quad (10)$$

Here $\epsilon_0 = f_t/E$ = strain at the strength limit; E = Young's modulus of concrete; f_t = tensile strength; ϵ_f = strain when stress σ is reduced to 0; and ϵ_k and σ_k are the stress and strain defining the knee point at

which the postpeak softening slope decreases abruptly. Denoting the crack band width as h (equal to the mesh size, given in Table 1), one may calculate ϵ_k and σ_k from G_f and G_F as follows:

$$\sigma_k = \frac{2}{h}\left(\frac{G_F - G_f}{\epsilon_f - (2G_f/f_t h)}\right),$$

$$\epsilon_k = \frac{2G_f}{f_t h} - \frac{\sigma_k}{f_t}\left(\frac{2G_f}{f_t h} - \epsilon_0\right) \quad (11)$$

As proposed in Mazars and Pijaudier-Cabot (1989), the tensile strain magnitude is a scalar defined as:

$$\kappa = \epsilon_{eq} = \sqrt{\sum_{i=1}^{3}\langle\epsilon_i\rangle^2} \quad (12)$$

where ϵ_i are the magnitudes of the principal strain vectors. The damage may grow only if $\epsilon_{eq} > \kappa$. In the present case of beams, $\epsilon_{eq} \approx \epsilon_1$.

The test results reported in Hoover et al. (2013) were optimally fitted with the bi-linear cohesive softening law shown by the curve in Fig. 3. The total area under this curve represents the total fracture energy G_F (RILEM Recommendation TC 50-FMC 1985; Nakayama 1965; Tattersall and Tappin 1966; Hillerborg 1985) and the area under the initial steeply

descending initial tangent represents the initial fracture energy G_f (Bažant and Pfeiffer 1987; Bažant and Kazemi 1991). The maximum loads of concrete structures depend almost exclusively on G_f, while G_F controls the postpeak response and energy absorption capability of structures. Note that, for the linear and exponential softening laws, the ratio G_F/G_f cannot be independently controlled, which is a major drawback of these laws.

To suppress spurious localization of damage and avoid mesh size sensitivity, the crack band model is adopted (Bažant 1982; Bažant and Oh 1983; Bažant and Planas 1998). The strain-softening curve for the crack band model is characterized by strains $\epsilon_k = w_k/h$ at the knee point (abrupt change in slope) and $\epsilon_f = w_f/h$ at the point where the stress across the band is reduced to 0; and h is the width of softening band, which is the same as the element size h. The width of the softening crack band, which is the same as the finite element size h and is, as the reference case, considered equal to the effective width w_f of the FPZ (which is best defined as the closest possible spacing of parallel cracks and is a feature missing from the cohesive crack model). In concrete, h is of the order of the maximum aggregate size, d_a, which is 10 mm here. When the element size is varied, spurious mesh sensitivity and localization instability are avoided by scaling the postpeak stress-strain relation so as to preserve energy dissipation per unit area of central crack plane. In the present numerical simulations, the ratio h/d_a varies from less than 1 to larger than 1 as the beam size increases (see Table 1), and the postpeak stress-opening relation is scaled accordingly. The stress–stress relations of the cohesive crack model exhibit no snapback for any size used in the experiments (the load-displacement relation, of course, does exhibit a snapback, but instability is avoided by controlling the relative displacement at the crack mouth, both in the tests and in the simulations).

The material parameters E, v, ϵ_0, G_F, G_f and w_k were specified independently. Their values corresponding to the optimum data fit are given in Table 2. From these values, the remaining materials parameters were calculated; they are $f_t = 3.92$ MPa, $\sigma_k/f_t = 0.15$, $G_F/G_f = 1.42$, $w_1 = 0.0253$ mm and $w_f = 0.0948$ mm.

It was also tried to fit the present data using a linear cohesive softening law and with Hillerborg's softening exponential law. However, none of these laws allowed

Table 2 Material parameters used for all simulations

| Parameter	Value
E	41.24 GPa
v	0.17
ϵ_0^*	0.000095
G_f	49.56 N/m
G_F^*	70 N/m
w_k^*	0.021505 mm

All data were taken directly from Hoover et al. (2013) and Hoover and Bažant (2013), except those marked with a superscript* which were calibrated to fit the simulations to the data

an acceptable fit of the present data because these softening laws have a fixed ratio of G_F/G_f. This represents a further proof that the bilinear softening law is a fundamental property of concrete (probably the same is true of all quasibrittle granular composites and geomaterials).

4 Results of finite element data fitting with the crack band model or equivalent cohesive crack model

The optimum fits of the measured curves of nominal strength σ_N versus the crack opening displacement δ_{CMOD} (Hoover et al. 2013) are displayed in Fig. 4. The thin solid curves represent the data mean and the maximum and minimum envelopes. Figure 5 shows the damage parameter ω in and around the ligament at the end of test for the beam depth of 93 mm and $\alpha = 0.3$. The solid black elements are completely damaged ($\omega = 1$). The gradient from white to black indicates increasing strain levels, and the damage zone is contained only within the width of one element, i.e., within the black elements, while the elements on the side of this zone are undamaged, i.e., remain elastic.

Through the entire range of data, the best-fit curves closely follow the experimental curves. The nominal strength σ_N for each relative notch depth was calculated using the classical bending strength equation $\sigma_N = M\bar{y}/I = M(D/2)/I$ where $M = P_u S/4 =$ maximum bending moment, $I = bD^3/12 =$ centroidal moment of inertia, and $\bar{y} =$ distance from the centroid to the tensile face of the beam; see Table 3. Figures 6 and 7 show the size effect, the plots of measured crack length effect and the simulation predictions of speci-
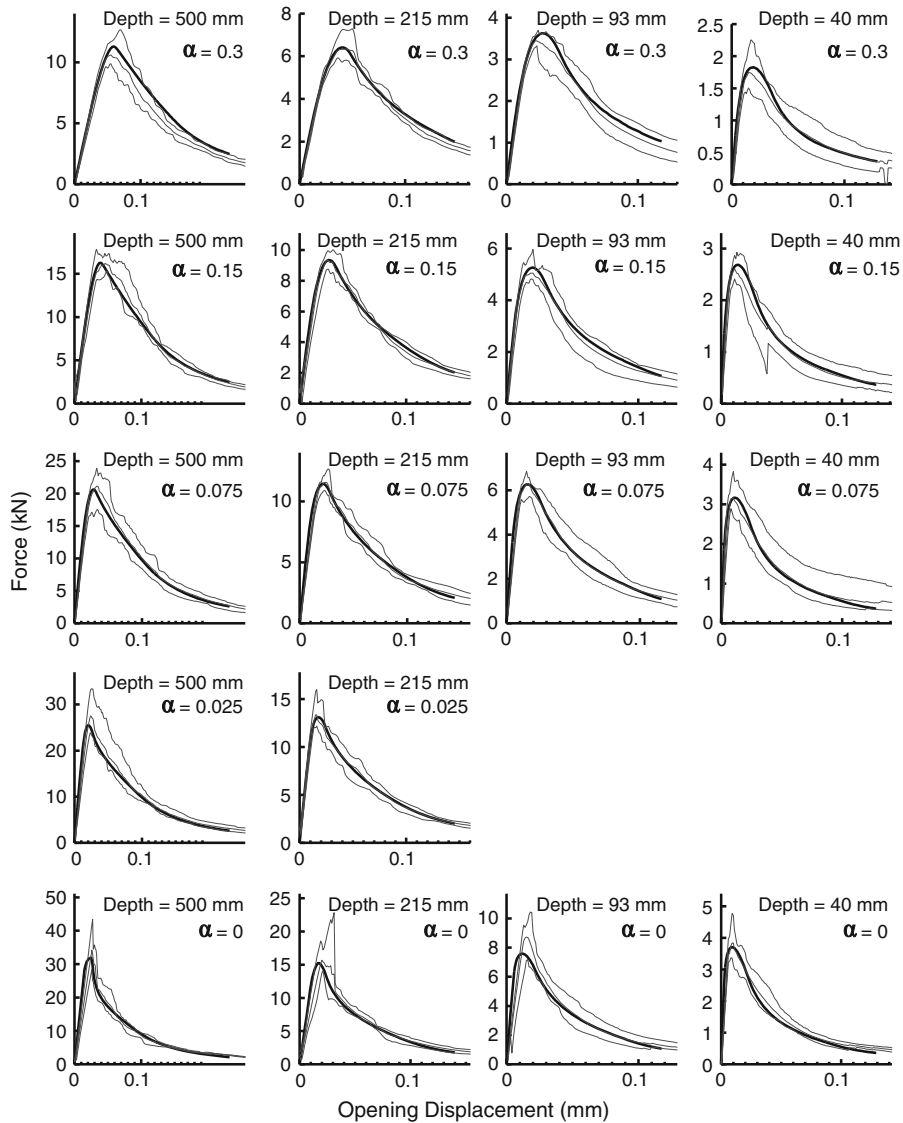
Fig. 4 The graphs of force versus opening displacement for the entire collection of beams (the *darker lines* are the simulation results and the *thin lines* are the maximum and minimum envelopes, and the average curves

men strength for each geometry. When the propagating crack approaches the top of the beam, the opening of the concrete elements in the upper ligament is prevented by connection to the nodes of the stiff elements of the steel loading block. This causes the softening to revert to hardening, and at that moment the simulation is terminated.

In view of the previous conclusion about nonuniqueness of the data fitting when the postpeak data are missing (Bažant and Yu 2011), it should be emphasized that what makes the present values of G_F and

G_f unambiguous is the knowledge of the postpeak response. The ratio of G_F/G_f in this study is equal to 1.4, which is smaller than the ratio previously obtained in Hoover et al. (2013), which was about two. The difference is not unexpected because the analysis in Hoover and Bažant (2013) determined G_F by the Hillerborg method (Hillerborg 1985) and considered only the geometries where $\alpha = 0.3$ and $\alpha = 0.15$. The present investigation matches the complete post-peak response from all beam geometries tested in (Hoover et al. 2013).
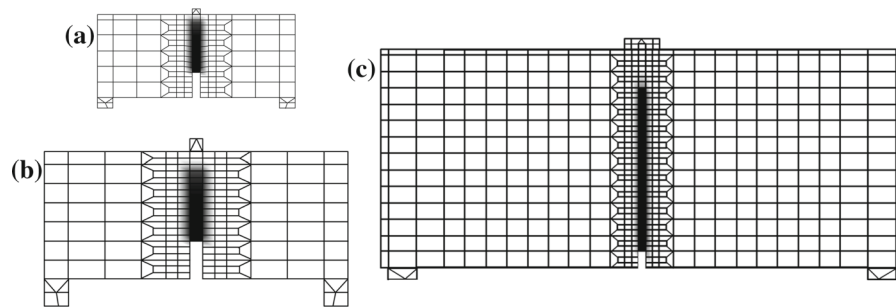
Fig. 5 Distribution of damage in the ligament at the end of softening for a specimen whose geometry is **a** D =40 mm and $\alpha = 0.3$, **b** D =93 mm and $\alpha = 0.3$ and **c** D =215 mm and $\alpha = 0.075$. The *solid black* elements have been completely damaged ($\omega = 1$) and the *solid white* elements are undamaged ($\omega = 0$). The gradient from *black* to *white* is a transition between completely damaged and undamaged

Table 3 Comparison of mean nominal strength values obtained from tests, calculated from calibrated USEL and from the optimum fits by cohesive crack model

α	Depth (mm)	σ_N (MPa)		
		Tests	USEL	Simulation
0.3	500	1.88	1.88	1.90
0.15	500	2.93	2.77	2.77
0.075	500	3.63	3.50	3.44
0.025	500	4.71	4.56	4.21
0	500	5.96	5.90	5.40
0.3	215	2.55	2.57	2.50
0.15	215	3.68	3.70	3.63
0.075	215	4.59	4.45	4.38
0.025	215	5.32	5.56	5.10
0	215	6.30	6.46	5.99
0.3	93	3.04	3.24	3.08
0.15	93	4.54	4.57	4.47
0.075	93	5.49	5.47	5.33
0	93	7.35	7.17	6.44
0.3	40	3.55	3.75	3.69
0.15	40	5.38	5.45	5.35
0.075	40	6.69	6.61	6.33
0	40	7.76	7.84	7.50

5 Comparison with universal size effect law and comprehensive fracture tests

The material values in Table 2 were used in the (non-statistical) USEL (Eqs. 6, 8) to determine the strength for all beam geometries. For all the relative notch depths, the strength values determined from the USEL closely match those obtained from the crack band simulations (equivalent to cohesive crack simulations) as well as the mean strength values from the comprehensive fracture tests; see Table 3. The G_f can then be calculated by fitting Eq. 3 to the σ_N values from either the USEL or from the crack band simulation fits with $\alpha = 0.15$ and $\alpha = 0.3$. The trust-region-reflective optimization algorithm (Coleman and Li 1994, 1996) was used to solve for G_f for these two geometries.

The optimization algorithm was also run jointly for $\alpha = 0.30$ and 0.15 (with different g_0 and g_0' for each), to fit Eq. (3) to both geometries simultaneously. In all cases, the G_f determined from either the simulations or the USEL gave almost exactly the same value; see Table 4. The small differences in G_f, visible in the figures, most likely occurred because of numerical errors, and because the USEL includes the effects of parameters governing the Type 1 size effect law which is irrelevant for fracture energy identification.

6 Conclusions

1. The finite element simulations of the comprehensive fracture tests using the crack band model with bilinear softening (which is virtually equivalent to the cohesive crack model) lead to excellent agreement with the measured peak loads and complete

Fig. 6 Effect of specimen size on the nominal strength of beams (the *hollow circles* are the means of test data and the *crosses* are the simulation predictions)
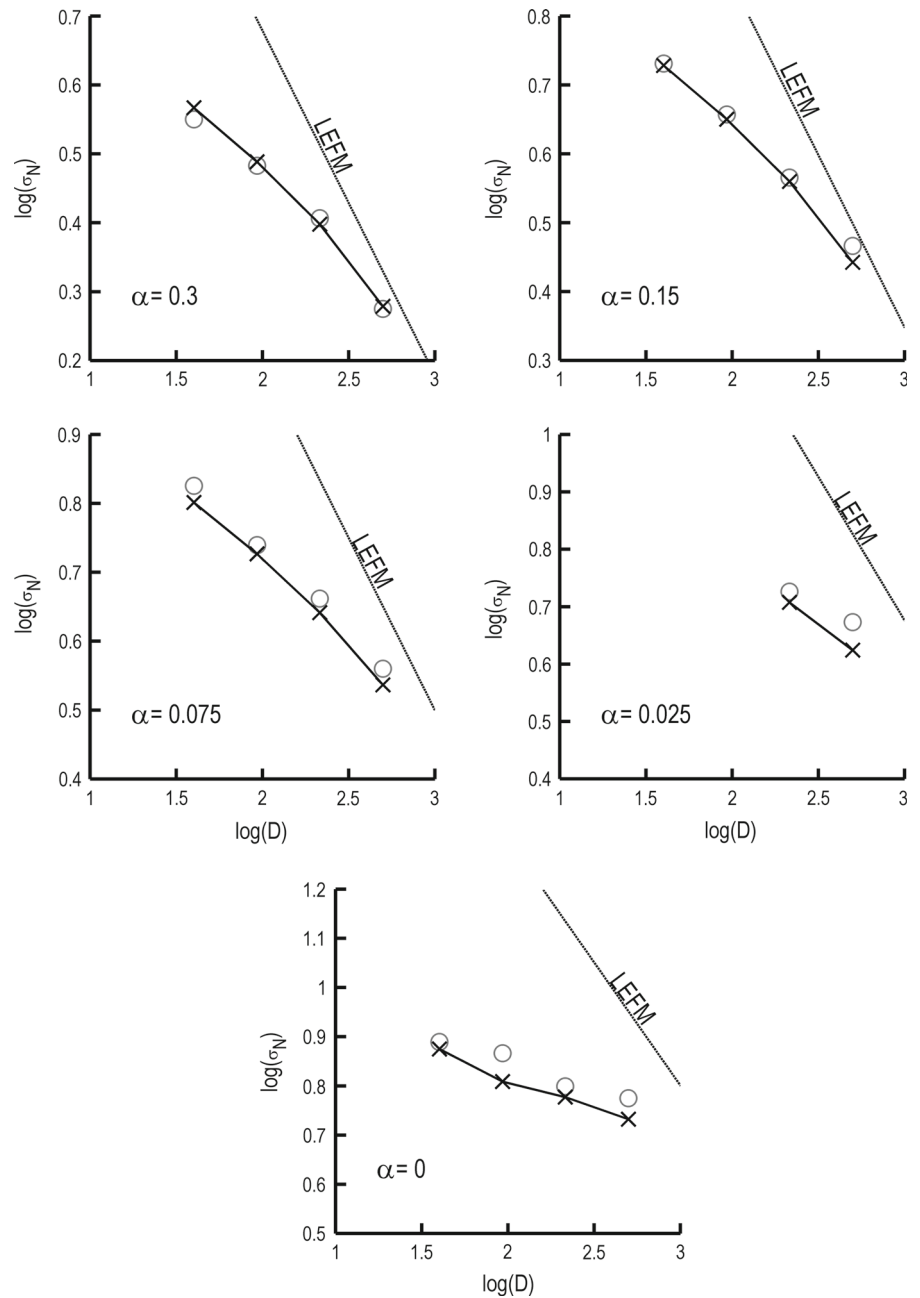

load-displacement curves for all the specimens of a broad size range (1:12.5) and notch depths ranging from 0 to 30% of beam depth. The same material fracture parameters have been used in all the fits.

2. The initial fracture energy G_f of the crack band model obtained by the finite element fitting of the test data is virtually the same as the G_f value obtained by the fitting the Type 2 size effect law simultaneously to the test data for both $\alpha = 0.3$ and $\alpha = 0.15$ relative notch depths, with different values of $g(\alpha)$ for each geometry.

3. The ratio of G_F/G_f for the concrete tested is 1.4. This value is unambiguous because it is the only one matching the complete post-peak responses of all the beams of all sizes.

Fig. 7 Effect of the relative crack length on the nominal strength of beams (the *hollow circles* are the means of test data and the *crosses* are the simulation predictions)
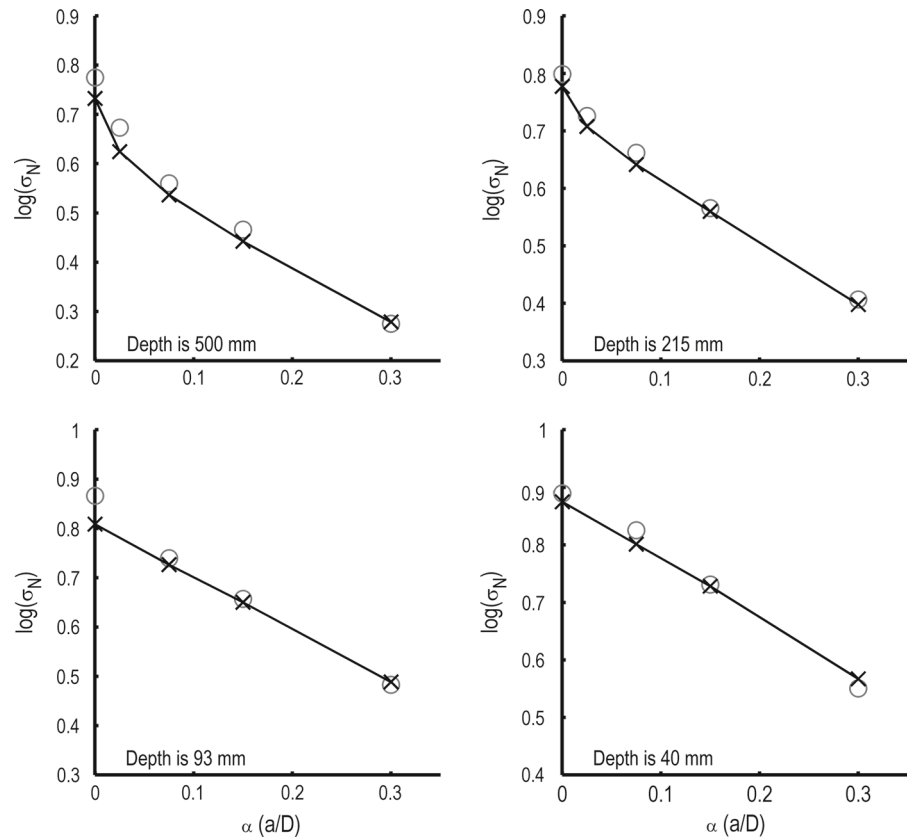
Table 4 G_f values calculated from strength values predicted from USEL and from simulations using material parameters in Table 2

α	G_f (N/m)	
	Simulation	USEL
0.15	44.73	45.42
0.3	47.85	49.49
0.15 and 0.3	45.36	46.51

4. The present test data cannot be fitted if the linear softening law or the Hillerborg exponential law is used.

References

Bažant ZP (1982) Crack band model for fracture of geomaterials. In: Proceedings of the 4th international conference on numerical methods in geomechanics, University of Alberta, Edmonton, (ed). by Eisenstein Z, held at University of Alberta, Edmonton, vol 3, pp 1137–1152

Bažant ZP (1984) Size effect in blunt fracture: concrete, rock, metal. ASCE J Eng Mech 110(4):518–535

Bažant ZP (1996) Size effect aspects of measurement of fracture characteristics of quasibrittle material. Ad Cem Based Mater 4(3/4):128–137

Bažant ZP (2005) Scaling of structural strength. Elsevier, MA, Burlington

Bažant ZP, Becq-Giraudon E (2002) Statistical prediction of fracture parameters of concrete and implications for choice of testing standard. Cem Concr Res 32(4):529–556

Bažant ZP, Kazemi MT (1991) Size dependence of concrete fracture energy determined by Rilem work-of-fracture method. Int J Frac 51:121–138

Bažant ZP, Li Z (1996) Zero-brittleness size-effect method for one-size fracture test of concrete. J Eng Mech 122(5):458–468

Bažant ZP, Novák D (2000) Energetic-statistical size effect in quasibrittle failure at crack initiation. ACI Mater J 97(3):381–392

Bažant ZP, Oh BH (1983) Crack band theory for fracture of concrete. Mater Struct 16:155–177

Bažant ZP, Pfeiffer PA (1987) Determination of fracture energy from size effect and brittleness number. ACI Mater J 84:463–480

Bažant ZP, Planas J (1998) Fracture and size effect in concrete and other quasibrittle materials. CRC Press, Boca Raton

Bažant ZP and Yu Q (2004) Size effect in concrete specimens and structures: New problems and progress In Fracture mechanics of concrete structures. In: Proceedings of fraMCoS-5, 5th international conference on fracture mechanics of concrete and concrete structures, Vail, Colo., vol 1, Li VC, Leung KY, Willam KJ, and Billington SL, (eds)., Swets and Zeitlinger, Balkema, Lisee, The Netherlands, 153–162

Bažant ZP, Yu Q (2009) Universal size effect law and effect of crack depth on quasi-brittle structure strength. J Eng Mech 135(2):78–84

Bažant ZP, Yu Q (2011) Size-effect testing of cohesive fracture parameters and nonuniqueness of work-of-fracture method. J Eng Mech 137(8):580–588

Coleman TF, Li Y (1994) On the convergence of reflective newton methods for large-scale nonlinear minimization subject to bounds. Math Prog 67(2):189–224

Coleman TF, Li Y (1996) An interior, trust region approach for nonlinear minimization subject to bounds. SIAM J Optim 6:418–445

Cusatis G, Schauffert EA (2009) Cohesive crack analysis of size effect. Eng Frac Mech 76:2163–2173

Carpinteri A, Chiaia B, Ferro G (1995) Multifractal scaling law: An extensive application to nominal strength size effect of concrete structures, No. 50. Atti del Dipartimento di Ingegneria Strutturale, Politecnico de Torino, Italy

Hillerborg A (1985) The theoretical basis of a method to determine the fracture energy g_f of concrete. Mater Struct 18:291–296

Hoover CG, Bažant ZP (2013) Comprehensive concrete fracture tests: Size effects of types 1 and 2, crack length effect and postpeak. Eng Frac Mech 110:281–289

Hoover CG, Bažant ZP (2014) Comparison of Hu-Duan boundary effect model to size-shape effect law for quasibrittle fracture based on new comprehensive fracture tests. J Eng Mech. doi:10.1061/(ASCE)EM.1943-7889.0000632

Hoover CG, Bažant ZP (2014) Universal size-shape effect law based on comprehensive concrete fracture tests. J Eng Mech. doi:10.1061/(ASCE)EM.1943-7889.0000627

Hoover CG, Bažant ZP, Vorel J, Wendner R, Hubler MH (2013) Comprehensive concrete fracture tests: description and results. Eng Frac Mech 114:92–103

Irwin GR (1958) Fracture. In: Flgge S (ed) Handbuch der physik. Springer, Berlin, pp 551–590

Karihaloo BL, Abdalla HM, Xiao QZ (2003) Size effect in concrete beams. Eng Frac Mech 70:979–993

Mazars J (1984) Application de la mécanique de l'endommagement au comportement nonlinéaire et à la rupture du béton de structure Thèse de doctorat d'etat, univ. vi, france, EPFL, Lausanne

Mazars J, Pijaudier-Cabot G (1989) Continuum damage theory-application to concrete. J Eng Mech 115(2):345–365

Malvar JL, Warren GE (1988) Fracture energy for three-point-bend tests on single-edge-notched beams. Exp Mech 28(3):266–272

Nakayama J (1965) Direct measurement of fracture energies of brittle heterogeneous material. J Am Ceram Soc 48(11):583

Nallathambi P (1986) Fracture behaviour of plain concretes. PhD thesis, Doctoral dissertation, University of New Castle, Australia

Patzák B, Bittnar Z (2001) Design of Object Oriented Finite Element Code. Ad Eng Softw 32(10–11):759–767

Petersson PE (1981) Crack growth and development of fracture zone in plain concrete and similar materials. Report no. tvbm-1006, Division of Building Materials, Lund Institute of Technology, Lund, Sweden

RILEM Recommendation TC 50-FMC (1985) Determination of the fracture energy of mortar and concrete by means of three-point bend tests on notched beams Mat. and Str., 18:285–290

Rocco CG (1995) Size dependence and fracture mechanisms in the diagonal compression splitting test. Phd thesis, Department of Ciencia de Materiales, Universidad Politecnica de Madrid

Sabnis GM, Mirza SM (1979) Size effect in model concretes. J Struct Div ASCE 105:1007–1020

Tang T, Bažant ZP, Yang S, Zollinger D (1996) Variable-notch one-size test method for fracture energy and process zone length. Eng Frac Mech 53(3):383–404

Tattersall HG, Tappin G (1966) The work of fracture and its measurement in metals, ceramics and other materials. J Mater Sci 1(3):296–301

Weibull W (1939) The phenomenon of rupture in solids. In: Proceedings of Royal Swedish Institute of Engineering Research, 153:1–55, Ingenioersvetenskaps Akad, Handl., Stockholm

Weibull W (1951) A statistical distribution function of wide applicability. J Appl Mech 18:293–297

Yu Q, Le JL, Hoover CG, Bažant ZP (2010) Problems with hu-duan boundary effect model and its comparison to size-shape effect law for quasibrittle fracture. J Eng Mech 136(1):40–50